Measurement of the Complex Index of Refraction for UO_x in the Extreme Ultraviolet

Heidi Dumais

Department of Physics and Astronomy, Brigham Young University

Abstract - The reflectance and transmittance in the extreme ultraviolet (XUV) for a diode sputtered with a uranium dioxide film (approximately 20 nanometers thick) were measured. The reflectance data for the coated side has been fit to the Parratt model in order to determine the thickness of the film. Fitting the transmission data to a simple model and combining this with the thickness calculation from the reflectance data yielded an estimate for the complex part of the index of refraction for uranium dioxide in the XUV region at every tenth of a nanometer in wavelength. The values will be further refined by a more robust analysis of both the reflectance and transmission data which the BYU XUV research group is currently undergoing. These values provide researchers with information for modeling, design and fabrication of optical systems in the extreme ultraviolet.

I. Introduction

Light incident on a material can be transmitted, reflected, or absorbed. An expression for the intensity of light reveals which parts of the index of refraction affect reflection and absorption:

$$e^{\frac{4\pi i}{\lambda}(1-\delta+\beta i)t} \qquad (1)$$

where 1-δ is the real part of the index of refraction, and β is the imaginary part. From Equation (1), the complex part of the index of refraction gives rise to an attenuation factor which corresponds to absorption. The real part of the index of refraction would affect the intensity of the reflected fields. The real and imaginary parts of the index of refraction depend on the wavelength of light incident on the material.

Most materials, including air, strongly absorb extreme ultraviolet (XUV) light which ranges from 1 – 60 nm. This range of wavelengths is also highly sensitive to surface roughness and contamination. Additionally, the real part of the index of refraction for materials in this region of the spectrum lies near unity for many materials, meaning that they don't reflect the light very well either. As a result, mirrors in this region must be constructed of layers of thin films with precise thicknesses meant to cause constructive interference between reflected fields from each interface. Figure 1. 1 shows a schematic for light incident on a three layer stack of thin films (on the nanometer scale) with reflectance at each interface. The beams which emerge from the top layer can add destructively or constructively. The thickness of each film will determine which.

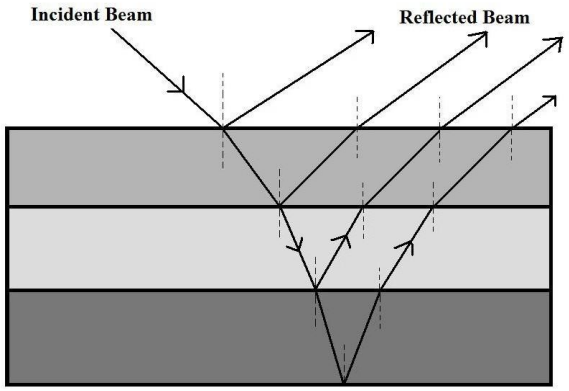

Figure 1. 1: Reflection of light from thin film interfaces.

The motivation for studying materials in the XUV includes integrated circuit applications, astrophysical observations, planetary physics, and high resolution microscopy. Photolithography techniques for microelectronics involve masks over photo-sensitive materials. The use of shorter wavelength light in this process increases the resolution dramatically, leading to smaller features and faster circuits. In astrophysics it becomes interesting and important to study objects in many light ranges, including XUV. Energetic processes which emit XUV light can be studied in greater detail

as better optics are developed in that range. In planetary science, helium ions trapped in the earth's magnetic field radiate in the XUV. As a result, images and movies of the earth's magnetic field have been made using XUV optics in satellites. In optical microscopy having a shorter wavelength leads to better resolution of smaller samples, with less preparation than that of electron microscopes. Understanding the optical properties of materials in the XUV allows for the design and fabrication of optical systems which can be used for all of these applications, in addition to a better understanding of the materials themselves.

II. Background And Calibration

We measured two samples at Lawrence Berkeley National Laboratory's Advanced Light Source (ALS). Both samples were uranium sputtered onto a silicon diode with a 7.69 nm SiO_2 layer. However, the first sample was sputtered in the presence of oxygen while the other was allowed to oxidize after sputtering. In both cases half of the diode was covered by a shutter to leave it uncoated for comparison.

To calibrate the measurements made at ALS the response of the uncoated part of the diode was compared to the standard measured by the ALS beamline personnel. Using MatLab, the normalized signal was given a wavelength offset to minimize the squared difference between the calibration curve and what we measured. The resulting wavelength shift, .0038 nm, was subtracted from each wavelength measurement made. This value made very little difference, as the precision of our wavelength measurements was only .01 nm.

After calibration measuring the reflectance and transmission of the sample at various wavelengths provides data for the calculation of the index of refraction of the sample material. Measurements of the transmitted intensity are made at a set wavelength by varying the angle of incidence of the beam. Each successive run has a different wavelength, so that analysis of each run yields the index of refraction at each wavelength. The reflection runs also have a constant wavelength for each run, and vary the incident angle. The measurements go from near grazing to near normal.

III. Analysis

The reflectance measured from near grazing to near normal yields an intensity curve which varies by several orders of magnitude. These curves show peaks and valleys in the reflectance measurement due to interference between fields which were reflected at the various thin film interfaces on the diodes. Figure 1. 1 shows a graphic depiction of how light incident on the top surface can be reflected at several interfaces and yield a more intense reflected beam than would be possible with a single material layer. The type of interference between these beams will depend on the index of refraction of each material (and hence the wavelength of light) and the thickness of the thin films. As a result, it should be possible to use the reflectance at various angles to determine the thickness of the layers.

The samples were prepared to have an approximate thickness of 20 nm. However, in order to find a more precise thickness, the reflectance data was fit to the Parratt recursive method including a Nevot-Croce correction factor for the surface roughness by varying the real and imaginary index of refraction and the film thickness in MatLab. The thickness of the SiO_2 layer was held constant at the measured value of 7.69 nm based on ellipsometry performed on the diodes at the BYU campus. The dramatic changes in reflectance during a single run result in the need for a weight function to prevent the optimization program from over or under emphasizing any one portion of the data. Figure 3. 1 through Figure 3. 6 show reflectance data fit to the Parratt model at various wavelengths. The plots include the weight function, the data and the fit curve. The average thickness of the UO_x layer for these runs was $21.8 \pm .7$ nm for the sample allowed to oxidize after sputtering, and $27.4 \pm .4$ nm for the sample which was sputtered with oxygen. These thicknesses allowed for a first approximation of the complex index of refraction based on analysis of the transmission data.

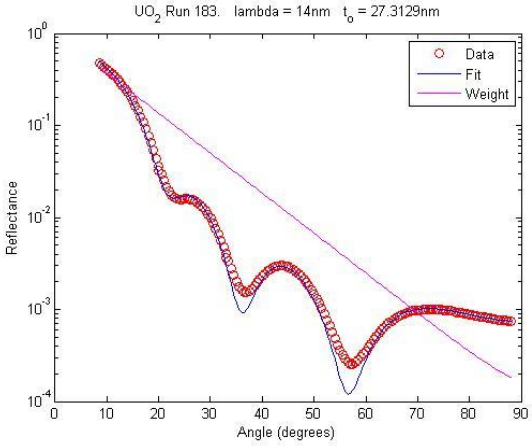

Figure 3. 1: Reflectance data fit to Parratt model for sputtered U allowed to oxidize.

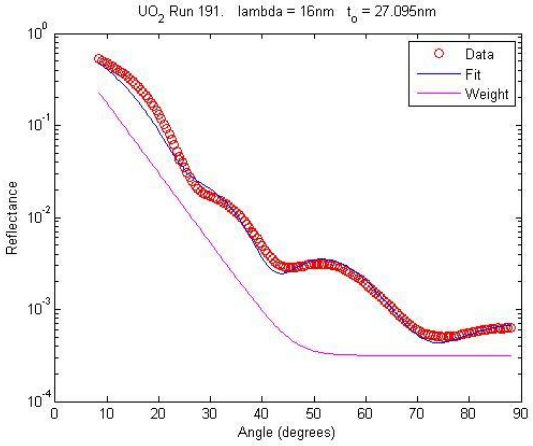

Figure 3. 2: Reflectance data fit to Parratt model for sputtered U allowed to oxidize.

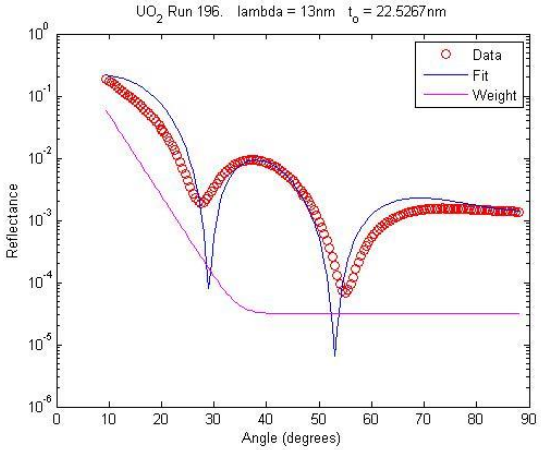

Figure 3. 3: Reflectance data fit to the Parratt model for U sputtered in the presence of oxygen.

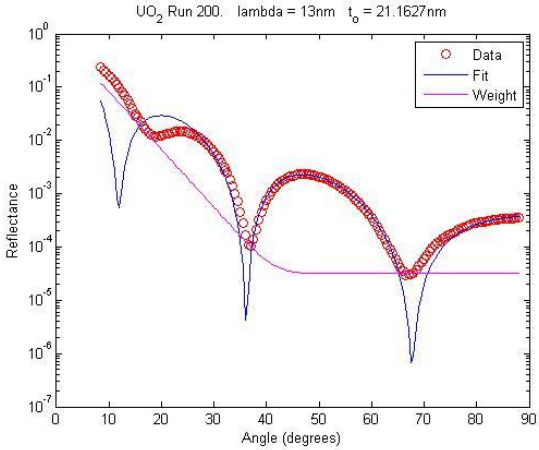

Figure 3. 4: Reflectance data fit to the Parratt model for U sputtered in the presence of oxygen.

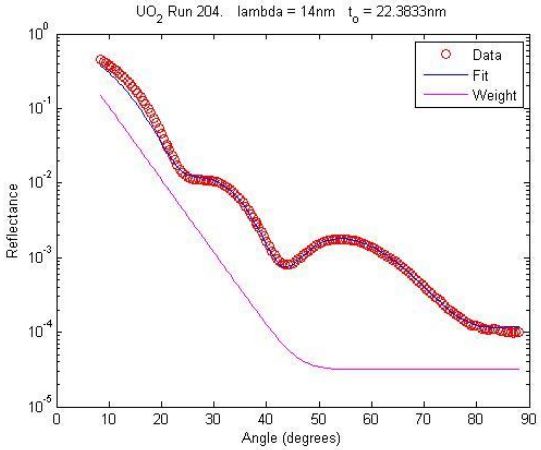

Figure 3. 5: Reflectance data fit to the Parratt model for U sputtered in the presence of oxygen.

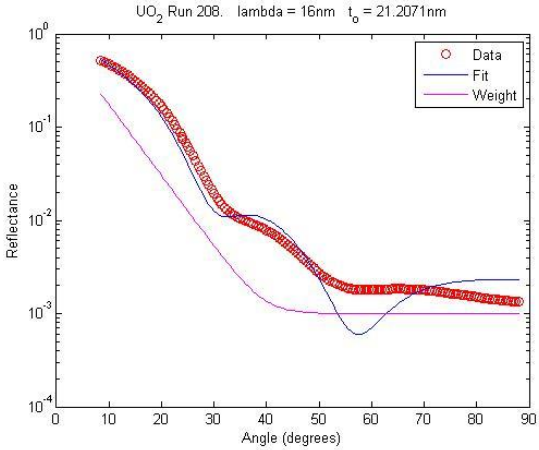

Figure 3. 6: Reflectance data fit to the Parratt model for U sputtered in the presence of oxygen.

Measurement of the transmission as a function of angle at a given wavelength (ranging from 1 nm to 40 nm in varied increments depending on the level of interest for each region) provided the data for the determination of the complex index of refraction. As a first approximation, the transmission current was assumed to be of the form

$$I = I_0 \xi e^{-\alpha t} \qquad (2)$$

where I is the measured current, I_0 is the incident current, ξ is some factor which will account for reflection, gunk on the surface, and surface roughness, t is the distance the light travels through the sample, and θ is the angle measured from grazing. Figure 3. 7 shows a cross section of the sample with these parameters.

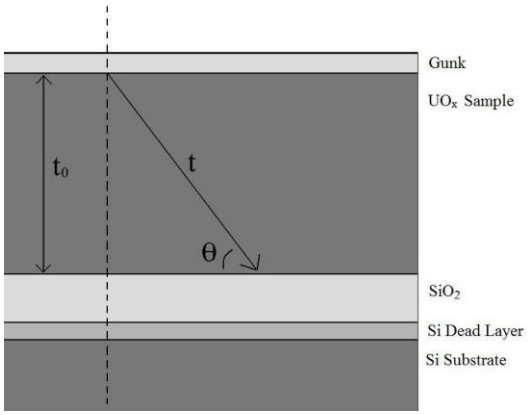

Figure 3. 7: Geometry of transmission approximation.

The variable t is given by

$$t = \frac{t_0}{\sin\theta} \qquad (3)$$

θ here assumes perfect sample alignment and t_0 is the film thickness. To correct for possible misalignment of the sample, we add another fitting parameter to theta and substitute the expression for t into Equation (2) to get

$$I = I_0 \xi e^{-\frac{\alpha t_0}{\sin(\theta+\phi)}} \qquad (4)$$

where ϕ corrects for the misalignment of the sample. Fitting the measured values to this model by varying the product of αt_0, ϕ, and the product of $I_0\xi$, we arrive at a value of αt_0 for each transmission run. If this model represents the data well, the value of ϕ for each run should be constant and close to zero since the sample was aligned the same way for each run and was very good. Figure 3. 8 shows ϕ for each run, and that it was relatively constant near zero.

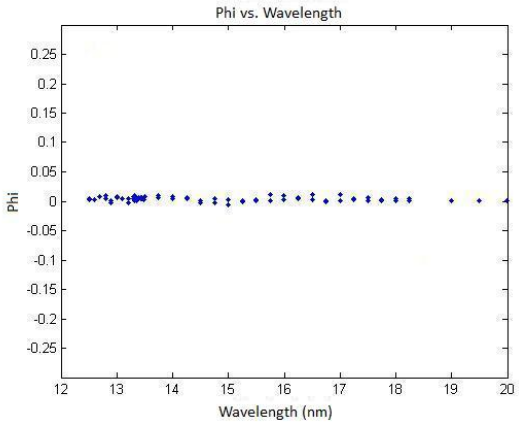

Figure 3. 8: Angle alignment correction for each run.

The reflectance analysis provided a value for t_0, the film thickness, allowing for the isolation of alpha. By comparing the attenuation factor we introduced to that acquired from an expression for the intensity of the field, Equation (1), we can arrive at an equation for β in terms of α,

$$\beta = \frac{\alpha\lambda}{4\pi} \qquad (5)$$

Using MatLab, we calculated a value for β at each wavelength according to the preceding analysis. Figure 3. 9 shows the results for the sample sputtered in the presence of O_2 and the sample which was allowed to oxidize after sputtering.

IV. Results

Figure 4. 1 compares the values predicted by the Center for X-Ray Optics (CXRO) for U, UO_2, U_3O_8 with both samples. The sample sputtered with O_2 seems to follow the U curve before dropping to the U_3O_8 values. The sample allowed to oxidize follows the values for U_3O_8. Comparison with silicon and silicon dioxide values indicates that they did not influence these measurements.

The analysis of the transmission data to arrive at the complex index of refraction ignored reflection, so a more robust and in depth analysis is required to confirm these results. Currently, the BYU

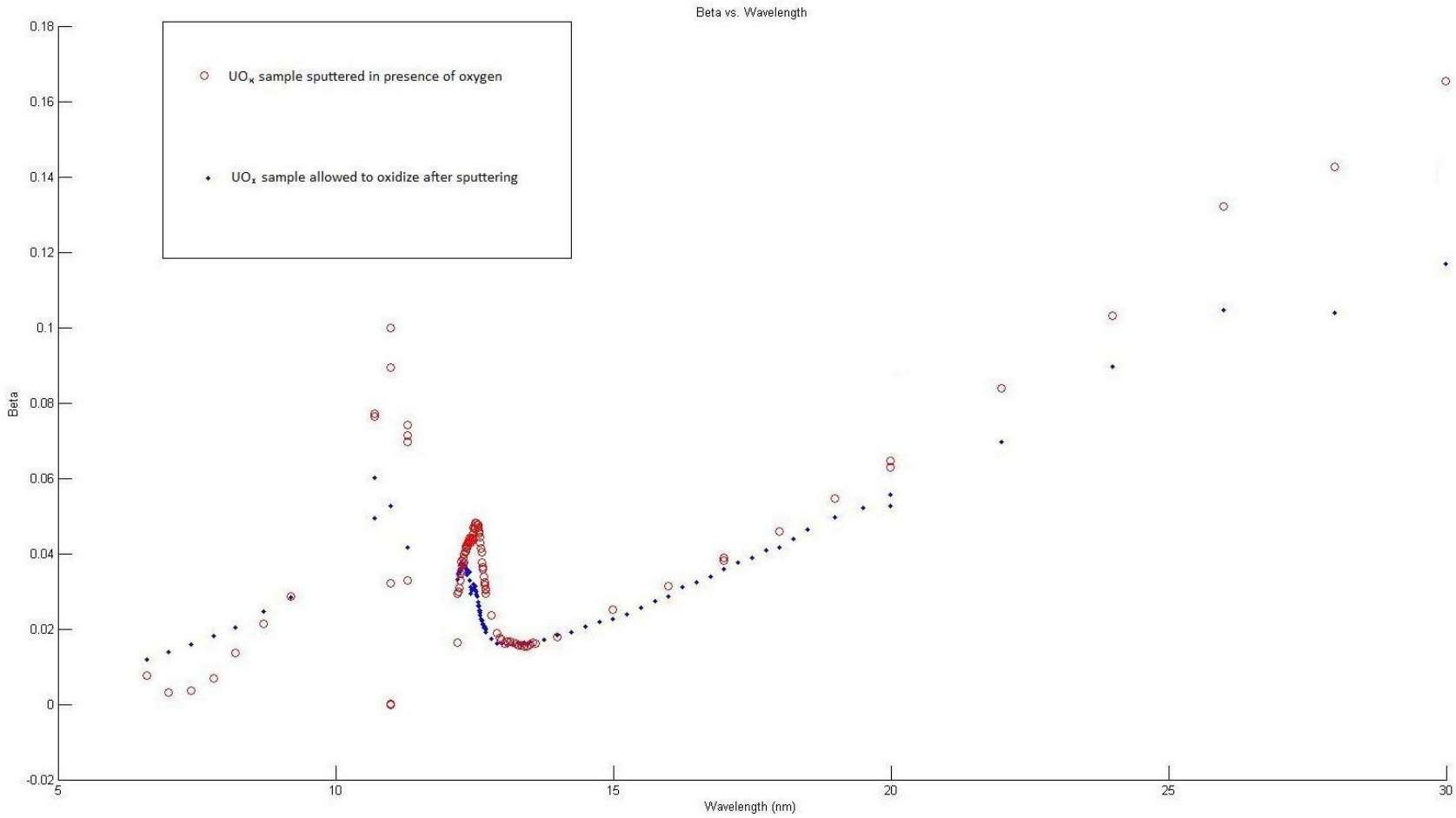

Figure 3. 9: Calculated complex index of refraction for sputtered UO_x samples.

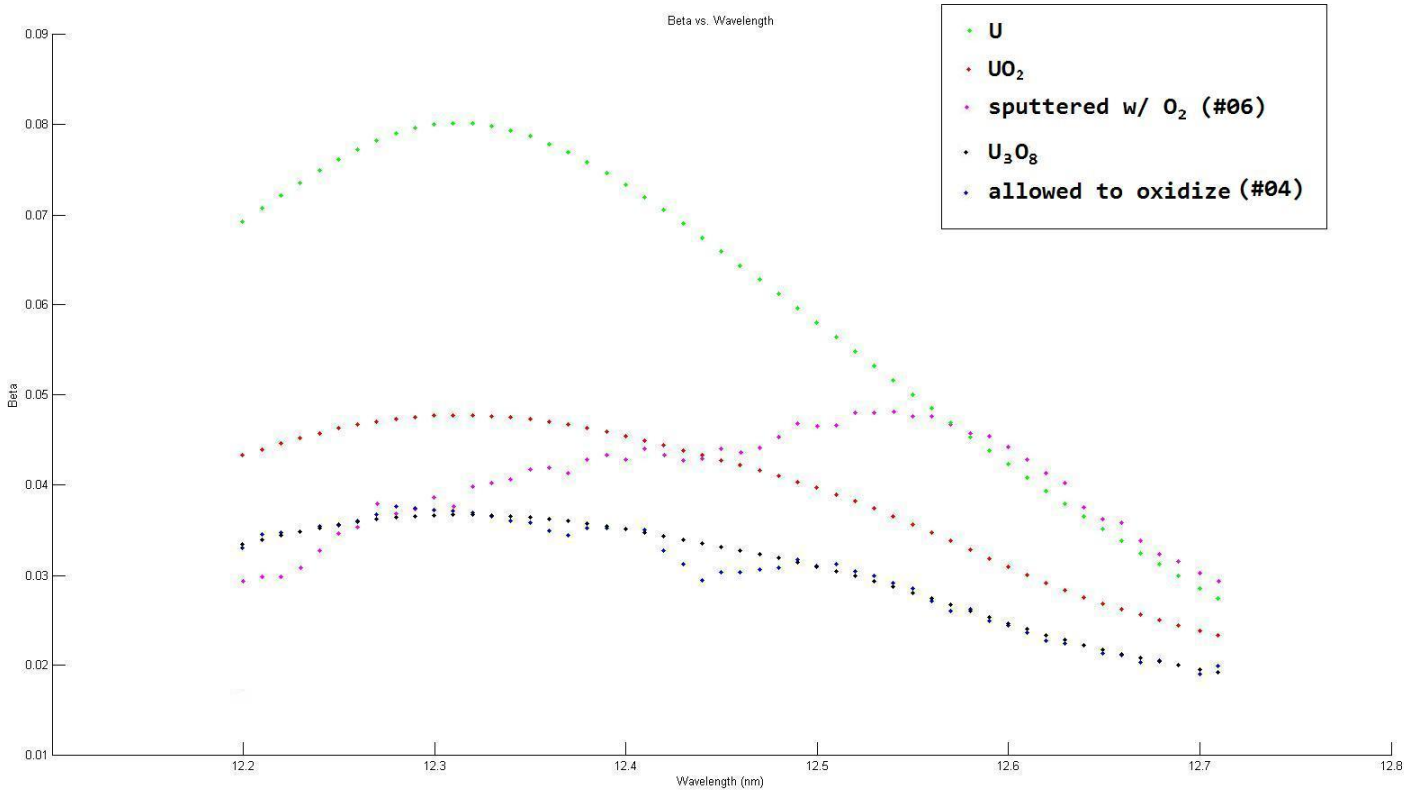

Figure 4. 1: Comparison of CXRO predicted complex indices with measured for both diodes.

XUV research group is writing MatLab code to take the transmission and reflection into account in order to find both the real and imaginary parts of the index of refraction for both samples. It will also be interesting to compare the results of the more robust calculation with the initial approximation of Equation (4) to see how accurate that model is.

VI. Conclusion

The complex index of refraction for UO_x has been measured for two different sample preparation procedures. The data indicates that the index of elemental uranium does influence the compound's index but not necessarily the same way as the CXRO predicts. Future research will refine these results and draw conclusions about the structure of the samples, and provide both the real and imaginary parts of the index of refraction for UO_x in the XUV range. These values will aid researchers in the modeling of XUV optical systems for application to photolithography, astronomical imaging, planetary science, high resolution microscopy, and materials characterization.

Acknowledgements

I would like to thank Dr. R. S. Turley and Dr. D. D. Allred for their help, patience and advice on this project, the Brigham Young University Physics and Astronomy Department for financial support and the use of their facilities, and DOE along with Eric Gullikson for the use of the ALS beamline. Additionally, I thank all of the undergraduate students who helped take measurements at the ALS, namely, Zephne Larsen, Keith Jackson, and Alison Wells